

# **Experiment Proposal for the Determination of Neutron Spectra from Targeted Electron Beams\***

**P. Degtyarenko and G. Stapleton,**

**Thomas Jefferson National Accelerator Facility† , Newport News, VA 23606**

## **Introduction**

There is a dearth of experimental data on the production and yields of neutrons from targeted electron beams; yet, for accelerator radiation protection these data are of the greatest importance in setting up methods of shielding and other means for protecting people against ionizing radiation (Nakashima 1995). Although adequate for simple cases and lateral production angles, empirical analytical methods are not suitable for the more complicated geometries or source configurations often met with in practice. Monte Carlo (MC) methods that model the transport of neutrons provide far better results in many cases but rely on the random generation of the energy of a source particle selected for any beam condition, production angle and target configuration. A number of theoretical approaches to the derivation of a model for the production of particle events at energies greater than the giant resonance region have been made. Many of these are based on the quasi deuteron model of the nucleus and operate over photon energies in the range 30 MeV to 400 MeV (Gabriel 1969, RCCC94). A method is also available, based on the vector meson dominance model which is designed to work above the photopion resonance region where the cross section levels off at a few GeV (Ranft 1987). Both of these models are limited in utility to a certain energy range and both show some discrepancies with existing empirical methods. More recently a new fragmentation model was developed, which could be used over a large energy range and modeled all production processes (Degtyarenko 1995). This new method also showed differences from the traditional approaches and a thorough comparison indicated that the event generator in conjunction with conventional MC transport codes produced results a factor two to three higher than the results using the empirical methods. This unsatisfactory situation can

---

\* Work supported by the U.S. Department of Energy under contract number DE-AC05-84ER40150.

† The Thomas Jefferson National Accelerator Facility (previously the Continuous Electron Beam Accelerator Facility - CEBAF) is informally called the Jefferson Laboratory (JLab). The existing accelerator facility at JLab is still referred to as CEBAF.

only be resolved by making measurements of proper physical quantities in the radiation field. Measurements of the angular fluence spectrum will permit a satisfactory resolution of the uncertainties surrounding the event generators and the transport codes. The conversion of the known energy fluence to the dose equivalent can then be dealt with by using an appropriate set of conversion coefficients. The measurement of the angular fluence spectrum is, however, not easy to do and this is particularly the case where interference from background radiation is high. The purpose of this paper is to describe a suitable spectrometer and discuss a suitable experiment which will answer many of the questions touched on above.

### **Scope of Experiment**

When an electron beam hits a target, complex products including hadronic and  $e,\gamma$  radiation results - all of this radiation has to be considered in radiation protection. The  $e,\gamma$  processes are well characterized but this is not so in the case of hadron production, furthermore, the  $\gamma A$  cross sections are very small (for  $eA$  they are smaller still) and both are strongly varying functions of  $e,\gamma$  energy. These problems have resulted in the lack of the quality measurements of hadron production needed to support the existing fragile and incompletely tested theories mentioned in the introduction. With regard to the neutron energies that we need to study for shielding purposes, neutrons with energies greater than 15 MeV are of particular interest. Because it is unlikely that shielding thinner than, say, 1 m of concrete would be specified even for low intensity sources at JLab energies (few GeV), this means that the lower energy part of the source neutron spectrum will be removed early on in the shielding process leaving the "high" energy neutron part to continue propagating the neutron spectrum through the shield. This phenomenon is well illustrated by figure 1. Thus for shielding high energy accelerators the high energy neutron yield is of primary importance. However, there are requirements for providing a complete neutron yield spectrum and these occur for low energy accelerators (injectors etc.) and where studies have to be made of neutron streaming along penetrations and access ways in which the major contribution to personnel dose is carried by the "fast" neutron component. JLab presents an excellent opportunity to perform such measurements due to its energy range (0.8 -- 4.0 GeV), and unique continuous electron beam time structure, providing the lowest possible

background conditions. An ideal measurement set-up would permit the determination of the differential cross section  $d^2\sigma(\gamma A \rightarrow n X)/dE_n d\Omega$  as a function of the incident photon energy  $E_\gamma$  and secondary neutron energy  $E_n$  in the reaction:  $\gamma + A \rightarrow n + X$ ; (1). However, such a measurement is most difficult since it requires a tagged photon facility. From a practical standpoint, what is actually needed for determining the radiation environment around any beam loss point is the total neutron yield from an electron interaction with the target which includes all channels of production for both  $\gamma$ -A and  $e$ -A reactions at all energies in the  $e,\gamma$  shower. Therefore, we propose to measure neutron yields at different initial electron beam energies, different target materials and thicknesses, and at laboratory emission angles from 20 to 160 degrees to the initial beam direction, i.e. the inclusive neutron production differential cross section  $d^2\sigma/dE_n d\Omega$  for the reaction:  $e^- + \text{nuclear target} \rightarrow n + X$ ; (2). The estimates of the cross section of reaction (1) can be made using measurements at different beam energies and target thicknesses. The data obtained can be used directly in radiation environment calculations, and will provide a good set of reference points for theoretical models of nuclear fragmentation at high energies.

### **Measurement Technique**

As the electromagnetic background may be expected to be very high in electron experiments, there is a clear need for an experimental technique capable of distinguishing between the neutron and photon signals. Separation of  $n$ - $\gamma$  events based upon the measurement of fast and slow components of a signal from liquid scintillator (Moszynski et al. 1992) proved to be successful in measurements of neutrons at  $E_n$  up to 20 -30 MeV. Its applicability for the measurement of higher energy neutrons, under high background conditions is unclear. Another technique of  $n$ - $\gamma$  separation, using heterogeneous scintillator-Cherenkov detectors was first introduced by P. Degtyarenko, Yu. Efremenko and V. Gavrilov in 1987 (Degtyarenko 1987). The  $n$ - $\gamma$  separation ability of the detector is based on the fact that neutrons with energies up to 400-500 MeV are very unlikely to produce Cherenkov radiation in a medium, as the charged products of their interaction are relatively slow. At the same time, photons, interacting in a dense and transparent medium such as Plexiglas or scintillator, produce secondary  $e^+ - e^-$  pairs and electrons fast

enough to emit detectable Cherenkov light. The detector with a repeating scintillator-Cherenkov radiator structure, with separate collection of scintillator and Cherenkov light, is capable of  $n$ - $\gamma$  separation. The light collected from the scintillator part may be used to measure the time of flight, and the energy deposition in the detector, as in the case of a standard thick scintillator neutron time-of-flight (TOF) detector. The Cherenkov arm of the heterogeneous detector provides the information on the type of interacting particle. The prototype version of the detector designed, assembled, and tested at ITEP showed that the technique worked as intended. We are proposing to use such technique for an experiment at JLab. The neutron energy range we are interested in (15–400 MeV) coincides with the range of best  $n$ - $\gamma$  separation in this technique. A schematic 3-D view of the proposed Scintillation-Cherenkov Spectrometer (SCS) detector is shown in figure 2. The sensitive volume consists of a series of scintillator plates 15x15x0.5cm with a plastic Cherenkov radiator plate of the same size behind each scintillator. The light from the scintillator set of plates is collected by the two plastic light guides glued to the opposite ends (e.g. up and down) of the plates. All plates are wrapped in white and black paper to make the light collection more uniform, and to eliminate the light contact between the scintillator and Cherenkov plate sets. The Cherenkov light is collected by the other two (left and right) similar light guides. The light guides have optical contact with 5 in., photomultiplier tubes with photocathode diameter 120 mm (Hamamatsu) or 110 mm (Philips). The parabolic shape of the lightguides and the dimensions of the detector are determined by the need to focus the light, exiting the plates at the angle of total internal reflection, onto the photocathode. Other elements of the detector shown are the anti-coincidence scintillator counter in front of the sensitive volume used to cut off the events with charged particles coming from the target. A few mm thick lead filter in front of the detector would screen it from the low-energy electron and positron background in the experimental hall. The detector was modeled using the CERN detector simulation package GEANT including the neutron transport code CALOR and GCALOR interface. The light output in the scintillator arm was calculated using Birk factors for heavy charged particles, and is expressed in equivalent MeV (light emitted by the electron of corresponding energy). The emission and transport of the Cherenkov light in the detector was

also modeled in GEANT. Figure 3 shows a horizontal plane cut of the SCS detector, with an event of 10 MeV photon (dotted line) interacting in the detector, producing electrons and/or positrons which emit Cherenkov photons (solid lines). The photons are then traced through the detector until being absorbed in the medium or at the photocathodes. The quantum efficiency of the photocathode and the effective absorption lengths of Cherenkov photons in the light guides as functions of the photon wavelength are taken into account in the model. The modeled performance of the SCS detector is illustrated in figures 4 and 5. The interactions of the 4 GeV electron beam with a 0.5 mm ( $\approx 10\%$  rad. length) lead target were modeled using the GEANT+DINREG Monte Carlo code. The generated spectra of neutrons and photons exiting the target in the angular range  $20^\circ$ – $160^\circ$  were used as input to the SCS model, which simulated the detector responses. Figure 4 shows light output in the scintillator arm ( $E_S$ ) vs. time-of-flight for all generated events. The target to SCS detector distance is set at 6 m. TOF resolution is determined by the random position of the interaction point in the detector and the resolution of the PMT, which was modeled to be proportional to  $E_S^{-1/2}$  and set to 0.2 ns at  $E_S = 40$  MeV. Figure 4 shows that the number of photons interacting in the detector is large compared to the number of neutrons, and that the photon background would set the limits on the possibility of detection of high energy neutrons. An additional problem for neutron detection (not illustrated in the figure) would be presented by delayed energetic photons, produced by re-scattering and secondary interactions, and by the decay of long-lived resonances like K mesons. Figure 4 shows all events not taking into account the information from the Cherenkov arm of the detector. Figure 5 shows the same events but without any signal in the Cherenkov arm. In this case the photon interactions are strongly suppressed, keeping the neutron detection efficiency practically unchanged. The degree of photon suppression depends on the energy deposited in the interaction (therefore, the light output  $E_S$ ), as the average number of photoelectrons detected in the Cherenkov arm increases with increasing  $E_S$ . The efficiency of photon suppression as a function of  $E_S$  is shown in figure 6 for two modifications of the SCS detector: one with plate thickness 1 cm, and the other for 0.5 cm plates. The photon suppression efficiency  $\eta$  is defined as the ratio of the number of photons that give a specified light output in the scintillator arm  $E_S$  and produce more than a

specified threshold number of photoelectrons in the Cherenkov arm ( $N_{ph.e.} > 10$  in the figure) to the total number of photons, which give the same  $E_S$ . The figure indicates that the photon suppression is close to 1 (100%) for the events with high energy deposition ( $E_S > 10$  MeV). The suppression is also rather high (60%–70%) for lower energy depositions,  $E_S \approx 1$ –2 MeV. Figure 6 shows also that 0.5 cm plates are preferable to 1 cm, as they give opportunity to use lower  $E_S$  thresholds, with better detector efficiency for neutrons. Further decrease in the plate thickness would help even more in this respect, but at some point the plates become too thin to effectively transport light to the edges due to the large number of internal reflections. Using 0.5 cm plates would be a reasonable compromise. The neutron detection efficiency of the SCS detector depends strongly on  $E_S$  threshold. Figure 7 shows neutron detection efficiency as a function of neutron energy. Three dependencies are shown for different values of  $E_S$  threshold: 2.5, 5.0, and 7.5 MeV. Different thresholds may be applied for analyses of different neutron energies. We may conclude from the figure that the neutron detection efficiency of the detector is expected to be of the order of 10% in the energy range 15 MeV and higher.

### **Experimental Setup and Beam Conditions**

The criteria for the experimental setup are determined by the need to “map” the neutron production cross sections, covering all accessible beam energies at JLab from 0.8 to 6.0 GeV, nuclear targets from carbon to lead, and the range in production angles from forward ( $20^\circ$ ) to backward ( $160^\circ$ ) direction. The experiment would require setting up SCS detectors around the experimental target in one of the JLab experimental Halls. A possible setup in Hall C is shown in figure 8. A special low-frequency time structure of the electron beam will be required. The standard continuous wave operation at JLab makes the beam time structure a series of very short ( $\approx 2$  ps) microbunches, and with the laser gun frequency of 500 MHz one microbunch would be produced every 2 ns. The time-of-flight neutron measurements require the time interval between the microbunches of the order of 100 ns to avoid ambiguity in determining the start time. Such a beam time structure may be achieved in the accelerator by changing the frequency of the laser gun injection from 500 MHz to 10 MHz. Assuming a beam current at 150  $\mu$ A CW, we may expect an average beam current of 1  $\mu$ A, in the low-frequency mode. Estimates of the SCS

detector loads and statistical accuracy achievable in the experiment have been performed using a GEANT+DINREG MC simulation of the electron interactions in the nuclear targets. These estimates are just the model predictions and should be treated with caution. We believe that the MC calculations are valid within a factor 2-3. Figures 9, 10, 11, and 12 show the modeled estimates of neutron spectra and the statistical accuracy of the cross section measurements, using 1 hour runs at 1  $\mu$ A beam current hitting approximately 10% radiation length targets of lead and carbon, at the incident energies 4 and 1.6 GeV. The SCS detector efficiency was assumed to be 10%, roughly corresponding to 5 MeV  $E_s$  threshold. We may conclude from the figures that the setup parameters chosen give reasonable rates of neutron interactions in the detector, of the order of few hundred events per second, which is within the limits of the data acquisition system available at JLab (up to 1000 triggers/sec). The photon interactions could be triggered out to a large extent using the signal from the Cherenkov arm of the detector as anti-coincidence, and choosing appropriate value of  $E_s$  threshold.

### **Conclusions**

We note that the experiment does not require a long run time, as far as statistical errors are concerned. The accuracy of the final results will probably be determined by systematic errors. We envisage the necessity of a calibration experiment to measure the efficiency. Different sources of background can be investigated with the help of additional test experiments, such as with targets of different thickness, using different target-detector distances, using filters to separate and measure the background from re-scattered photons and neutrons, and measuring backgrounds due to the accidental coincidents.

### **Acknowledgments**

The authors wish to thank Bob May and Radiation Control Group at JLab for their help and support, and also Yuri Efremenko (UT/ORNL) for valuable discussions.

### **References**

Degtyarenko, P.; Efremenko, Yu.; Gavrilov, V. Scintillation - and - Cherenkov light heterogeneous detector for neutron detection in the kinetic energy range 50 - 300 MeV. In: Proceedings of the International Symposium on Coordinate Detectors. Dubna, USSR; 1988: 316-318.

Degtyarenko, P. Applications of the Photonuclear Fragmentation Model to Radiation Protection Problems. In: Shielding Aspects of Accelerators, Targets, and Irradiation Facilities (SATIF2). Proceedings of OECD Nuclear Energy Agency Second Specialist's Meeting. CERN, Geneva, Switzerland; October 1995: 67-91.

Gabriel, T. A. and Alsmiller Jr., R. G. Photonuclear disintegration at high energies ( $<350$  MeV). Phys. Rev. 181: 1035; 1969.

GCALOR. C. Zeitnitz and T. A. Gabriel, "The GEANT - CALOR Interface User's Guide" (1995).

GEANT User's Guide, CERN Program Library, Geneva, Switzerland (1994).

Moszynski, M. et al., DEMON Collaboration. Study of  $n - \gamma$  discrimination by digital charge comparison method for a large volume liquid scintillator. Nucl.Instrum. and Methods. A317: 262; 1992.

Nakashima, H. et al. Accelerator shielding benchmark experiment analyses. In: Shielding Aspects of Accelerators, Targets, and Irradiation Facilities (SATIF2). Proceedings of OECD Nuclear Energy Agency Second Specialist's Meeting. CERN, Geneva, Switzerland; October 1995: 115.

Ranft, J. and Nelson, W.R. Hadron cascades induced by electron and photon beams in the GeV range, Nucl. Instrum. and Methods. A257: 177; 1987.

RCCC94. PICA – Monte Carlo Medium-Energy Photon-Induced Intranuclear Cascade Analysis Code System, RSIC Computer CodeCollection, Documentation for CCC-160/PICA Code Package, Oak Ridge National Laboratory, Oak Ridge, Tennessee, 1994.

### Figure Captions

Figure 1. Neutron dose outside spherical concrete shield vs shield thickness. The dose is averaged over the polar emission angle  $\Theta$ . The source is a 20 cm copper target positioned in the center of the sphere and irradiated by a 4 GeV electron beam. The solid line shows the sum dose. Lines with symbols are the doses from neutrons in different energy intervals.

Figure 2. Schematic 3D view of the SCS detector.

Figure 3. Horizontal plane cut of the SCS detector.

Figure 4. Light output (equivalent MeV) in scintillator arm vs. time of flight (ns) for photons

(circles) and neutrons (squares). The target to detector distance is set to 6 m. All events. Solid line indicates the neutron kinetic energy corresponding to the TOF value. Neutrons with energies 20-50-100-200-400 MeV and more are shown with squares of different intensity (color). Photons with energies 2-5-10-20-50-100-200... MeV are shown with circles of different intensity.

Figure 5. Light output (equivalent MeV) in scintillator arm vs. time of flight (ns) for photons (circles) and neutrons (squares). The target to detector distance is set to 6 m. Events are shown with no photoelectrons detected in Cherenkov arm.

Figure 6. The efficiency of gamma suppression as a function of light output measured in scintillator arm. Circles: SCS model with plate thickness 0.5 cm; triangles: SCS model with plate thickness 1 cm.

Figure 7. The integral efficiency of neutron detection as a function of neutron kinetic energy. The threshold values 2.5, 5.0, and 7.5 MeV are shown.

Figure 8. Possible experimental setup for neutron spectra measurements at JLab Hall C. SCS detector(s) are shown at six positions at different neutron production angles and distances from the target. Schematic beam line equipment is shown including beam pipe, interaction chamber, and beam dump line (He-filled pipe).

Figure 9. Neutron kinetic energy spectra from 0.5 mm thick ( $\approx 10\%$  rad. length) lead target hit by 4 GeV electron beam. Lines show DINREG+GEANT calculations at different polar angles. Markers represent binning of the spectra approximately corresponding to the expected time-of-flight resolution of the detector (better than 0.5 ns standard deviation). The hatched areas show the expected statistical accuracy (standard deviation) in the bins, assuming 1 hour run at  $1\mu\text{A}$  beam current and detector efficiency 10%. The target to detector distances are varied from 6 to 3 meters as the polar angle changes from 20 to 160 degrees. The expected neutron detection rates are shown for each angle and distance setup. The two sets of horizontal lines illustrate the expected energy resolution corresponding to time-of-flight resolution 0.5 ns.

Figure 10. Same as in figure 9, for 1.6 GeV electron beam.

Figure 11. Same as in figure 9, for 4 GeV electron beam and 2 cm ( $\approx 10\%$  rad. length) carbon target.

Figure 12. Same as in figure 9, for 1.6 GeV electron beam and 2 cm ( $\approx 10\%$  rad. length) carbon target.

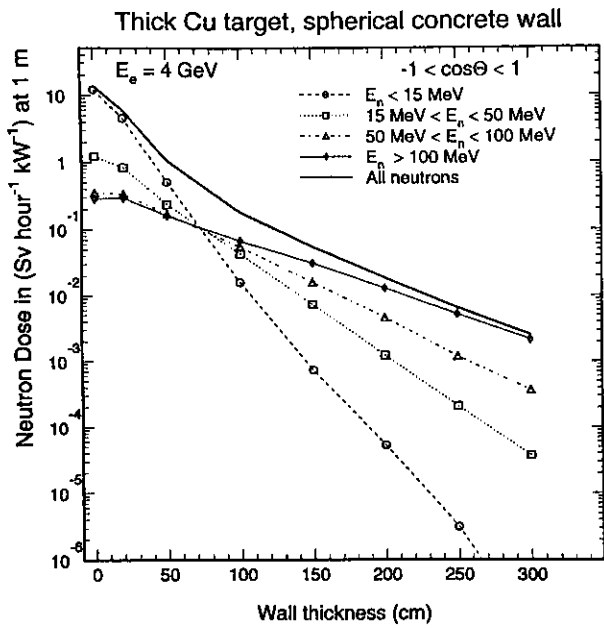


FIG. 1.

SCS Detector

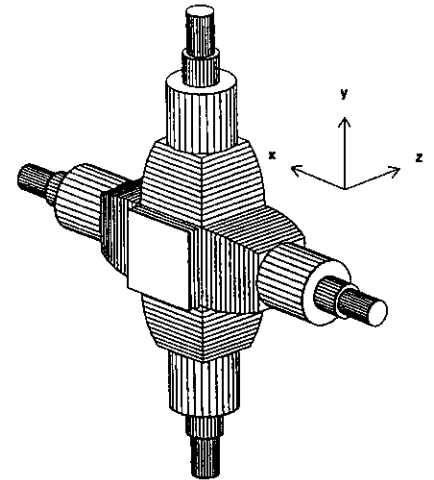


FIG. 2.

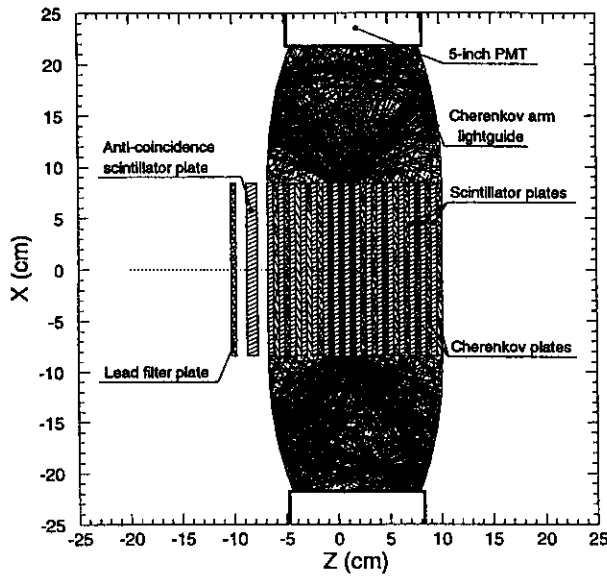


FIG. 3.

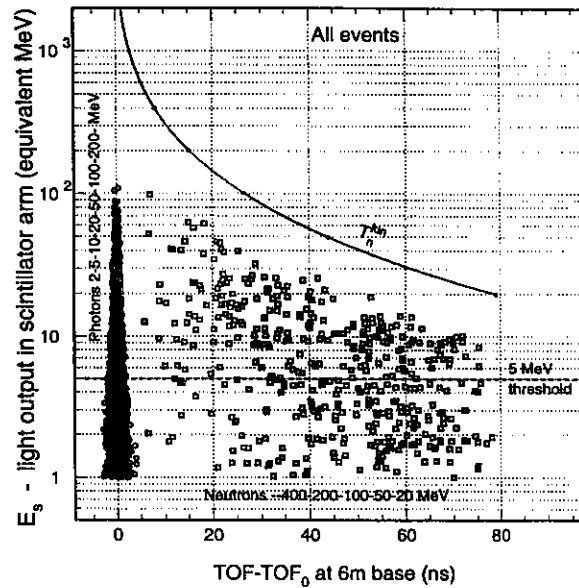


FIG. 4.

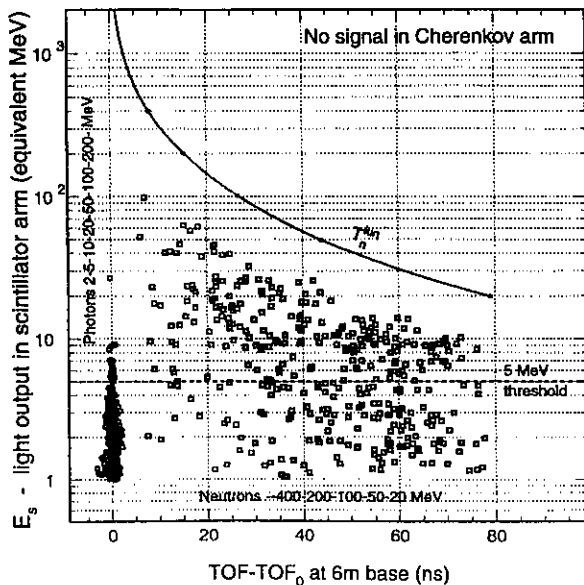


FIG. 5.

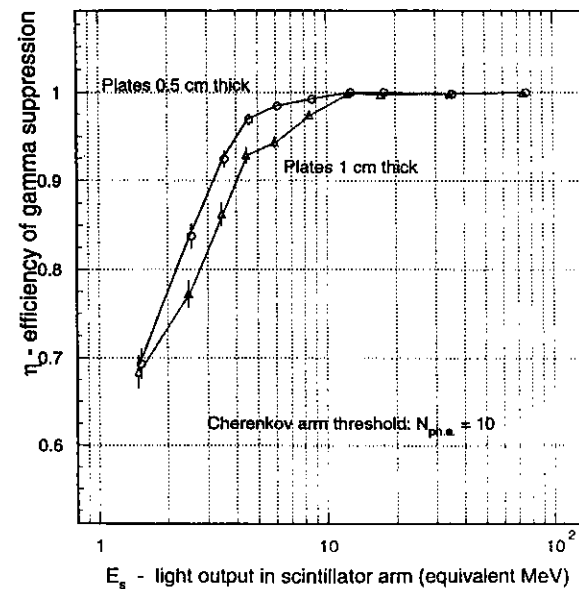


FIG. 6.

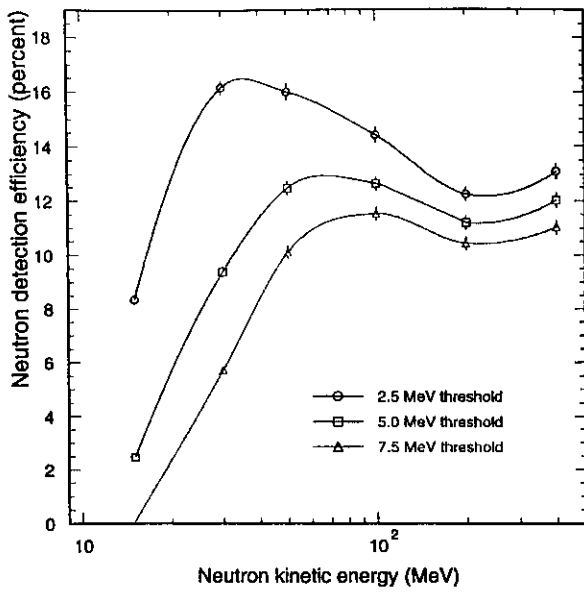


FIG. 7.

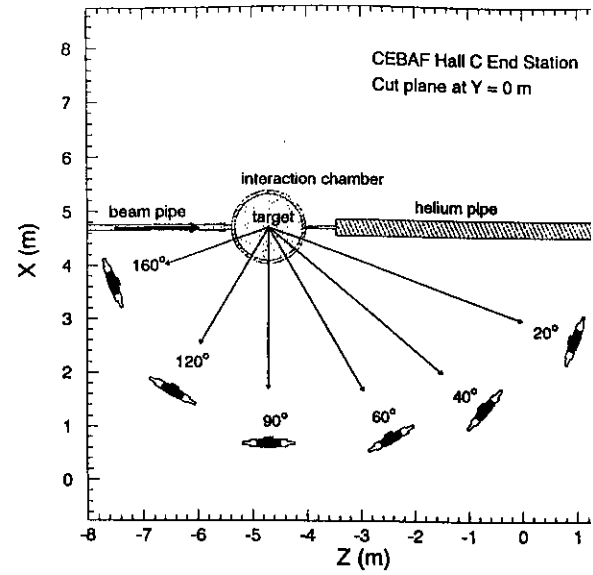


FIG. 8.

$e + \text{Pb} \rightarrow n + X$  at  $E_0 = 4 \text{ GeV}$  (0.05 cm target)

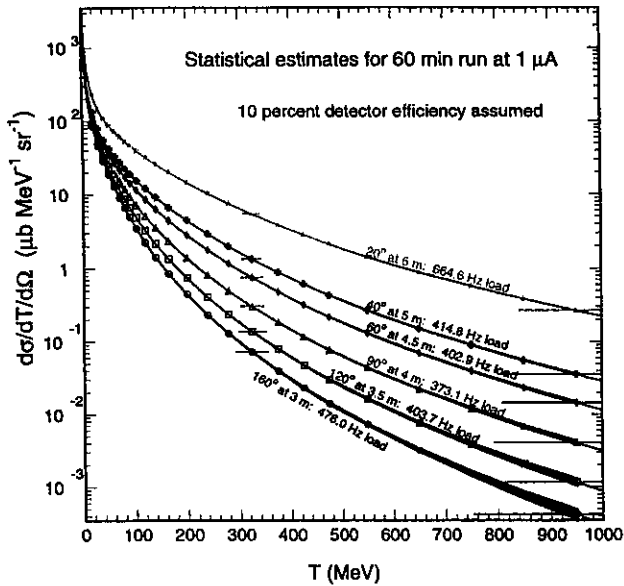


FIG. 9.

$e + \text{Pb} \rightarrow n + X$  at  $E_0 = 1.6 \text{ GeV}$  (0.05 cm target)

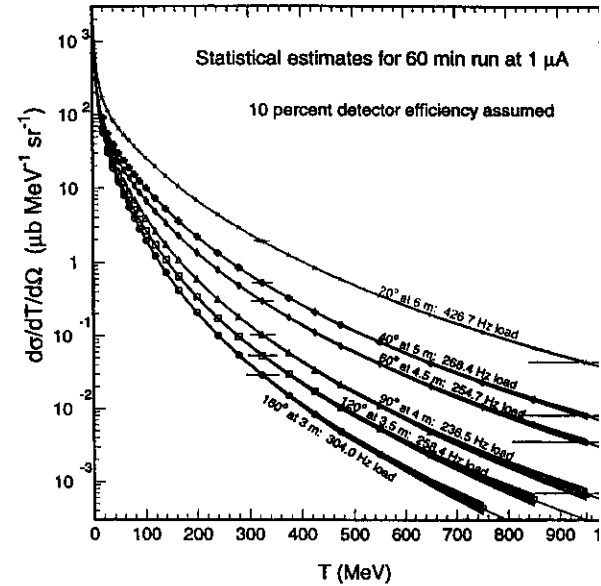


FIG. 10.

$e + \text{C} \rightarrow n + X$  at  $E_0 = 4 \text{ GeV}$  (2 cm target)

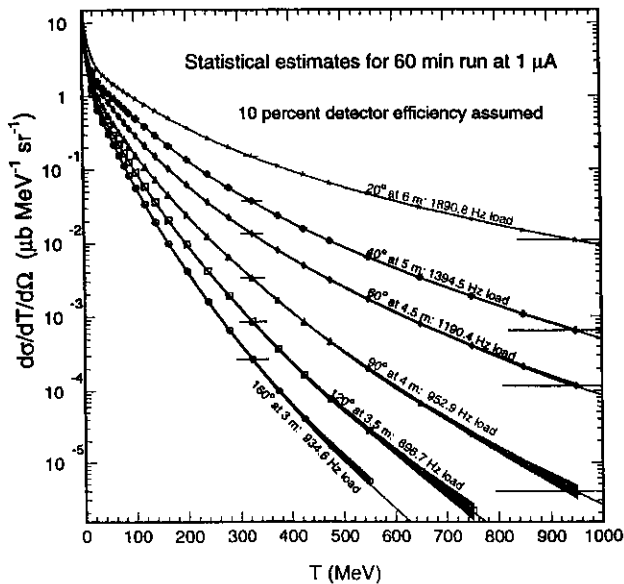


FIG. 11.

$e + \text{C} \rightarrow n + X$  at  $E_0 = 1.6 \text{ GeV}$  (2 cm target)

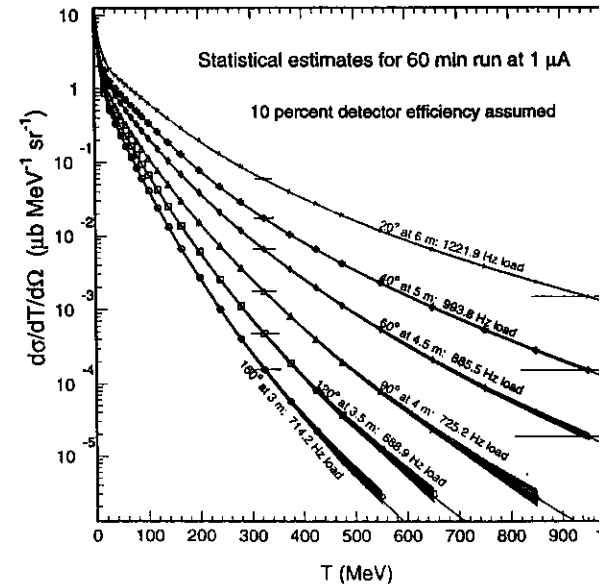


FIG. 12.